Available online at www.sciencedirect.com
SCIENCE DIRECT®
Journal of Solid State Chemistry 178 (2005) 2077–2090
JOURNAL OF SOLID STATE CHEMISTRY
www.elsevier.com/locate/jssc

Structure, magnetic properties and Mössbauer spectroscopy of GdRhSn

Kazimierz Łątka[a], Roman Kmieć[b], Robert Kruk[b], Andrzej W. Pacyna[b], Thomas Fickenscher[c], Rolf-Dieter Hoffmann[c], Rainer Pöttgen[c,*]

[a]*Marian Smoluchowski Institute of Physics, Jagiellonian University, Reymonta 4, 30-059 Kraków, Poland*
[b]*Henryk Niewodniczański Institute of Nuclear Physics, Polish Academy of Sciences, Radzikowskiego 152, 31-342 Kraków, Poland*
[c]*Institut für Anorganische und Analytische Chemie, Universität Münster, Corrensstrasse 36, D-48149 Münster, Germany*

Received 10 March 2005; received in revised form 7 April 2005; accepted 7 April 2005

Abstract

Polycrystalline GdRhSn was obtained by a reaction of the elements in a sealed tantalum tube in a high-frequency furnace. The sample was investigated by X-ray diffraction on powder and a single crystal: ZrNiAl type, space group $P\bar{6}2m$, $a = 752.6(1), c = 386.38(6)$ pm, w$R_2 = 0.0353$, 454 F^2 values and 14 variables. Both crystallographically independent rhodium atoms have a tricapped trigonal prismatic coordination, i.e. [Rh1Sn_3Gd_6] and [Rh2Sn_6Gd_3]. The shortest distances occur for the Rh–Sn contacts (274 and 283 pm). Together the rhodium and tin atoms build up a three-dimensional [RhSn] network in which the gadolinium atoms fill distorted hexagonal channels. The magnetic and electronic properties of GdRhSn have been studied by means of magnetic AC and DC susceptibility measurements as well as ^{119}Sn and ^{155}Gd Mössbauer spectroscopy. A transition from a paramagnetic to an antiferromagnetic state with non-collinear magnetic ordering takes place at $T_N = 16.0(1)$ K.

Keywords: Intermetallic compound; Magnetism; Mössbauer spectroscopy

1. Introduction

The ternary equiatomic rhodium stannides *RE*RhSn (*RE* = rare earth element) have intensively been studied with respect to their largely varying magnetic and electrical properties [1–26]. For the magnetic behavior of GdRhSn, different data have been reported. In an early publication by Dwight [1], fitting parameters for ^{119}Sn Mössbauer data at 295, 77.3, and 4.2 K have been presented. From broadening of the spectrum at 77.3 K with respect to the room temperature data Dwight assumed magnetic ordering already above that temperature. This, however, is in contrast to the antiferromagnetic ordering at $T_N = 14.8$ K reported by Routsi et al. [2].

In the course of our systematic studies on magnetic properties and ^{155}Gd Mössbauer spectroscopy (MS) of equiatomic Gd*TX* (*T* = transition metal; *X* = *s* or *p* element) intermetallics [27–31] we have investigated the structure and properties of GdRhSn in more detail. Gadolinium intermetallics play an important role since they can be treated as reference materials for isostructural intermetallics with other rare earths. Owing to the fact that Gd^{3+} has the $^8S_{7/2}$ electron configuration, compounds with gadolinium give the unique opportunity to study their magnetic behavior neglecting the influence of crystal field effects.

Herein, we report on detailed AC and DC susceptibility measurements and a ^{119}Sn and ^{155}Gd Mössbauer spectroscopic study. Some preliminary results of this work have been reported at a conference [32]. Special

*Corresponding author. Fax: +49 251 83 36002.
E-mail addresses: uflatka@cyf-kr.edu.pl (K. Łątka), pottgen@uni-muenster.de (R. Pöttgen).

0022-4596/$ - see front matter © 2005 Elsevier Inc. All rights reserved.
doi:10.1016/j.jssc.2005.04.010

attention was paid to give a consistent description of the complicated magnetic behavior that is present below the antiferromagnetic transition temperature.

2. Experimental

2.1. Synthesis

Starting materials for the synthesis of GdRhSn were gadolinium ingots (Johnson Matthey, distilled lumps), rhodium powder (Degussa-Hüls, 200 mesh), and a tin bar (Heraeus), all with purities better than 99.9%. In a first step, small gadolinium pieces were arc-melted to a small button under an argon pressure of ca. 600 mbar. The argon was purified before over titanium sponge (900 K), silica gel, and molecular sieves. The button was subsequently mixed with rhodium powder and pieces of the tin bar in the ideal 1:1:1 atomic ratio and arc-welded in a small tantalum tube (ca. 1 cm^3) under an argon atmosphere of about 800 mbar. The tantalum tube was placed in a water-cooled quartz glass sample chamber of a high-frequency generator (Hüttinger TIG 1.5/300) under purified flowing argon. Details on the arc-melting technique and the high-frequency setup are given in [33] and [34]. The tube was first heated for 1 min at 1500 K, cooled to about 1100 K and heated again to 1500 K, followed by annealing at 900 K for another 4 h and quenching by radiative heat loss within the sample chamber. The moisture stable sample was obtained in X-ray pure form in an amount of 1 g. For more details concerning the preparation of *RE*RhSn stannides we refer to a previous paper [14].

2.2. X-ray diffraction

The sample was characterized through its Guinier powder pattern using Cu$K\alpha_1$ radiation and α-quartz ($a = 491.30, c = 540.46$ pm) as an internal standard. The hexagonal lattice parameters (Table 1) were obtained from a least-squares fit of the powder data. The correct indexing of the pattern was ensured through an intensity calculation [35] taking the atomic positions from the structure refinement. The lattice parameters determined from the powder and the single crystal agreed well.

Single crystal intensity data were collected at room temperature by use of a four-circle diffractometer (CAD4) with graphite monochromatized Mo$K\alpha$ (71.073 pm) radiation and a scintillation counter with pulse height discrimination. The scans were taken in the $\omega/2\theta$ mode and an empirical absorption correction was applied on the basis of psi-scan data, followed by a spherical absorption correction. All relevant details concerning the data collection are listed in Table 1.

Table 1
Crystal data and structure refinement for GdRhSn

Empirical formula	GdRhSn
Molar mass (g/mol)	378.85
Unit cell dimensions (powder data)	$a = 752.6(1)$ pm $c = 386.38(6)$ pm $V = 0.1895$ nm^3
Calculated density (g/cm^3)	9.96
Crystal size (μm^3)	$10 \times 20 \times 40$
Transm. ratio (max/min)	0.894: 0.647
Abs. coefficient (mm^{-1})	41.8
$F(000)$	477
θ range for data collection	3° to 40°
Range in $h\,k\,l$	±13, ±13, ±6
Total number of reflections	3869
Independent reflections	454 ($R_{int} = 0.1097$)
Reflections with $I > 2\sigma(I)$	385 ($R_{sigma} = 0.0552$)
Data/parameters	454/14
Goodness-of-fit on F^2	0.999
Final R indices [$I > 2\sigma(I)$]	$R_1 = 0.0290$; w$R_2 = 0.0326$
R indices (all data)	$R_1 = 0.0447$; w$R_2 = 0.0353$
Flack parameter	0.04(2)
Extinction coefficient	0.0050(3)
Largest diff. peak and hole	1.89 and −2.06 e/Å^3

2.3. Structure refinement

Small, irregularly shaped single crystals of GdRhSn were examined by use of a Buerger camera equipped with an image plate system (Fujifilm BAS–1800) in order to establish both symmetry and suitability for intensity data collection. The isotypy with the hexagonal ZrNiAl type [36], space group $P\bar{6}2m$, was already evident from the X-ray powder data.

The atomic parameters of isotypic HoRhSn [14] were taken as starting values and the structure was refined using SHELXI-97 [37] (full-matrix least-squares on F^2) with anisotropic atomic displacement parameters for all atoms. Refinement of the Flack parameter [38,39] indicated the wrong absolute structure. We inverted the atomic parameters and refined the structure again. As a check for the correct composition and the correct site assignment, the occupancy parameters were refined in a separate series of least-squares cycles along with the displacement parameters. All sites were fully occupied within two standard deviations and in the final cycles the ideal occupancies were assumed again. The final difference Fourier synthesis was flat (Table 1). The positional parameters and interatomic distances of the refinement are listed in Tables 2 and 3. Further details on the structure refinement are available.[1]

[1]Details may be obtained from: Fachinformationszentrum Karlsruhe, D-76344 Eggenstein-Leopoldshafen (Germany), by quoting the Registry No. CSD–413353.

Table 2
Atomic coordinates and anisotropic displacement parameters (pm^2) for GdRhSn

Atom	Wyckoff site	x	y	z	U_{11}	U_{22}	U_{33}	U_{12}	U_{eq}
Gd	3*f*	0.59265(8)	0	0	79(2)	91(3)	89(2)	45(1)	85(1)
Rh1	2*d*	2/3	1/3	1/2	80(3)	U_{11}	118(6)	40(1)	93(2)
Rh2	1*a*	0	0	0	76(4)	U_{11}	194(9)	38(2)	116(3)
Sn	3*g*	0.2585(1)	0	1/2	83(3)	66(3)	99(4)	33(2)	85(2)

Note. U_{eq} is defined as one-third of the trace of the orthogonalized U_{ij} tensor. $U_{13} = U_{23} = 0$.

Table 3
Interatomic distances (pm), calculated with the lattice parameters taken from X-ray powder data of GdRhSn

Gd:	4	Rh1	299.0	Rh1:	3	Sn	283.3
	1	Rh2	306.6		6	Gd	299.0
	2	Sn	317.1	Rh2:	6	Sn	274.2
	4	Sn	330.9		3	Gd	306.6
	2	Gd	386.4	Sn:	2	Rh2	274.2
	4	Gd	395.2		2	Rh1	283.3
					2	Gd	317.1
					4	Gd	330.9
					2	Sn	337.0

Note. All distances within the first coordination sphere are listed. Standard deviations are all smaller or equal than 0.1 pm.

2.4. Scanning electron microscopy

The bulk sample and the investigated single crystal have been analyzed in a LEICA 420 I scanning electron microscope equipped with an Oxford EDX analyzer. Since the crystal was mounted by beeswax on a glass fibre, it has first been coated with a carbon film. GdF_3, Rh, and tin have been used as standards for the EDX measurements. The analyses (32 ± 2 at% Gd: 34 ± 2 at% Rh: 34 ± 2 at% Sn) were in good agreement with the equiatomic composition. The relatively large standard deviation accounts for the various point analyses. Also the bulk sample was carefully analyzed. No impurity elements such as tantalum from the crucible have been observed.

2.5. Magnetic measurements

The magnetization and the magnetic susceptibility measurements were carried out on a powdered sample by means of the Faraday method with a Cahn RG automatic electrobalance in the range of temperature $4.2\,K < T < 300\,K$ as well as using a Lake Shore 7225 AC Susceptometer/DC Magnetometer between 4.2 and 150 K. In the first case, the sample was placed in an inhomogeneous magnetic field with a constant value of $H_0 \partial H_0/\partial z$ (with $H_0 = 454$ Oe), while in the latter one the used magnetic field H_0 was homogeneous ranging up to 57.5 kOe. All magnetic measurements were started first using the zero-field cooling mode (ZFC), where the sample was initially cooled down in zero external magnetic field, while in the field cooled (FC) mode an external magnetic field was switched on above the transition temperature in the paramagnetic region. Temperature dependences of the complex AC magnetic susceptibility $\chi = \chi' - i\chi''$, where χ' is real and χ'' the imaginary component, were measured at different driving field frequencies f and depending on the amplitude of this field H_{AC}. In addition, for better characterization of the sample, the higher harmonics (i.e. the second χ_2, the third χ_3, and the fifth χ_5) were also investigated as a function of temperature.

2.6. Mössbauer spectroscopy (MS)

The ^{155}Gd and ^{119}Sn MS studies on GdRhSn were performed with a ^{155}Eu:$SmPd_3$ (86.5 keV γ transition) and a $Ba^{119}SnO_3$ (23.875 keV γ transition) source, respectively. A standard constant acceleration spectrometer of the Kankeleit type in transmission geometry was used. The velocity scale was calibrated at room temperature with a ^{57}Co(Cr) source and a metallic iron foil. Spectra were recorded in a liquid helium cryostat at temperatures between 4.2 and 20 K in the case of ^{155}Gd MS and in the range between 293 and 1.8 K for ^{119}Sn MS.

Absorbers were made of the fine powdered compound with an optimized [40,41] thickness equal to 254.2 and 26.8 mg/cm^2 for ^{155}Gd and ^{119}Sn MS measurements, respectively. Both resonance transitions were detected using a 3 cm thick NaI(Tl) scintillation counter. A 0.9 mm thick lead foil was applied as a critical absorber to suppress the intensity of the higher 105.3 keV γ-ray transition during ^{155}Gd measurements with the 86.5 keV γ line while a 0.05 mm palladium foil was used to reduced the background intensity of the recorded spectra caused by the 25.3 keV tin X-rays in the case of ^{119}Sn MS with the 23.875 keV γ resonance. The isomer shifts values are given relative to the source materials.

Since the gadolinium and tin sites have a rather low symmetry (*m*2*m*), i.e. two mutually perpendicular mirror planes, a complete hyperfine interaction

Hamiltonian [42] was used to determine the hyperfine parameters. The Hamiltonian was considered in the principal axis system of the electric field gradient (EFG) tensor:

$$\hat{H} = -g\mu_B H_{hf}\left[\hat{I}_z \cos\theta + \frac{1}{2}(\hat{I}_+ e^{-i\varphi} + \hat{I}_- e^{i\varphi}) \sin\theta\right] + \frac{\Delta E_Q}{4I(2I-1)}\left[3\hat{I}_z^2 - \hat{I}^2 + \frac{\eta}{2}(\hat{I}_+^2 + I_-^2)\right],$$

where H_{hf} is the magnetic hyperfine field at the nuclear site; $\Delta E_Q = eV_{zz}Q$ is the quadrupole interaction constant, V_{zz} is the z-component of the EFG tensor; and Q is the quadrupole moment of the nuclear state; η is the asymmetry parameter defined as $\eta = (V_{xx} - V_{yy})/V_{zz}$, θ is the angle between the direction of H_{hf} and the V_{zz}-axis; φ is the angle between the V_{xx}-axis and projection of H_{hf} onto the xy plane. If the principal axes are chosen in the form $|V_{xx}| < |V_{yy}| < |V_{zz}|$ then $0 \leqslant \eta \leqslant 1$.

A transmission integral formula was applied to describe the resonance lineshapes. For ^{155}Gd studies, the source linewidth Γ_S and the background reduced Debye–Waller factor f_S of the source were obtained from the independent measurement with a standard $GdFe_2$ absorber, where the natural linewidth $\Gamma_{nat} = 0.25$ mm/s [43] was assumed. The Debye–Waller factor f_A was fitted as an independent parameter. During the analysis, the g factor and the quadrupole-moment ratios were constrained as equal to $g_{ex}/g_g = 1.235$ and $Q_{ex}/Q_g = 0.087$, respectively [44]. The interference ξ factor for the $E_\gamma = 86.5$ keV γ transition in the ^{155}Gd nuclei was fixed to the value $\xi = 0.0275$ [42,45].

3. Results and discussion

3.1. Crystal chemistry

GdRhSn crystallizes with the ZrNiAl-type structure [36]. The structure contains two crystallographically independent rhodium sites which both have a tricapped trigonal prismatic coordination (Fig. 1, bottom). The shortest distances occur between the rhodium and tin atoms (274 and 283 pm). The Rh–Sn distances are only slightly longer than the sum of the covalent radii of 265 pm for rhodium and tin [46]. Together, the rhodium and tin atoms build up a three-dimensional [RhSn] network in which the gadolinium atoms fill distorted hexagonal channels (Fig. 1, top). Within this network the shortest Sn–Sn distances are 337 pm, significantly longer than in the structure of β-tin (4×302 pm; 2×318 pm) [47]. We can thus assume only weak Sn–Sn bonding. For further details concerning the crystal chemistry of the series of *RE*RhSn stannides we refer to [14].

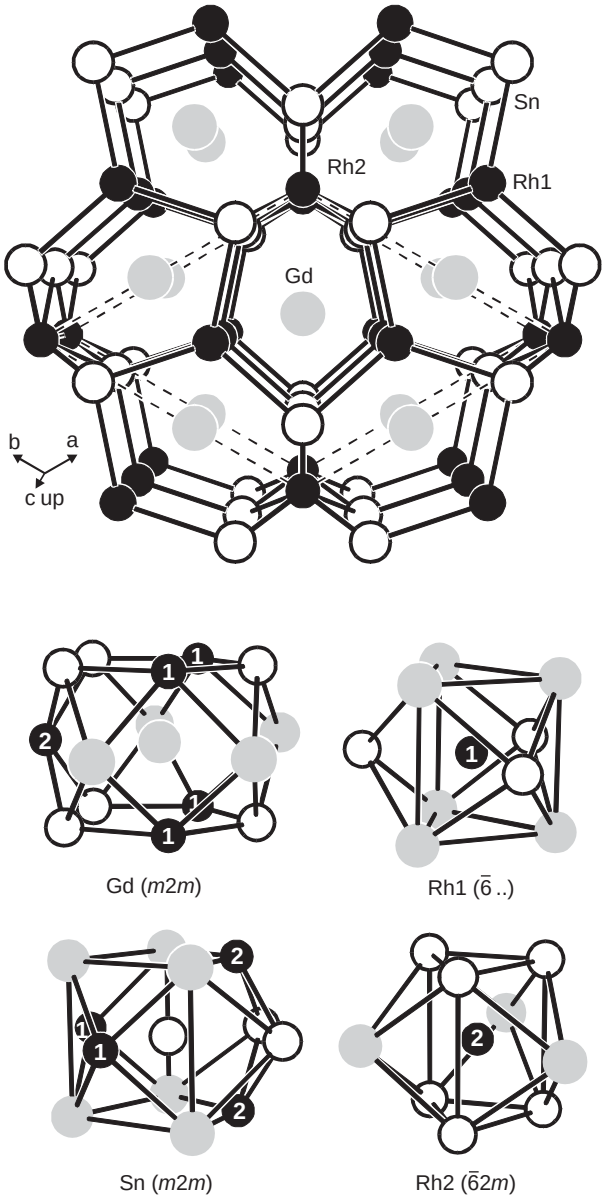

Fig. 1. The crystal structure of GdRhSn. The three-dimensional [RhSn] network is emphasized at the top and the coordination polyhedra (with site symmetries) are show at the bottom. The gadolinium, rhodium, and tin atoms are drawn as gray, filled, and open circles, respectively.

3.2. Magnetic properties

The results of magnetic measurements are displayed in Figs. 2–12. The static magnetic susceptibility temperature dependence obtained from balance measurements in a magnetic field of 454 Oe (Fig. 2) and its reciprocal show the behavior typical for a phase transition from a paramagnetic to an antiferromagnetic state at the Néel temperature $T_N = 16.0(1)$ K. Above 125 K, the recorded susceptibility obeys a modified Curie–Weiss law in the form $\chi_\sigma = \chi_0 + C/(T - \Theta_p)$ fairly well, with the temperature independent factor

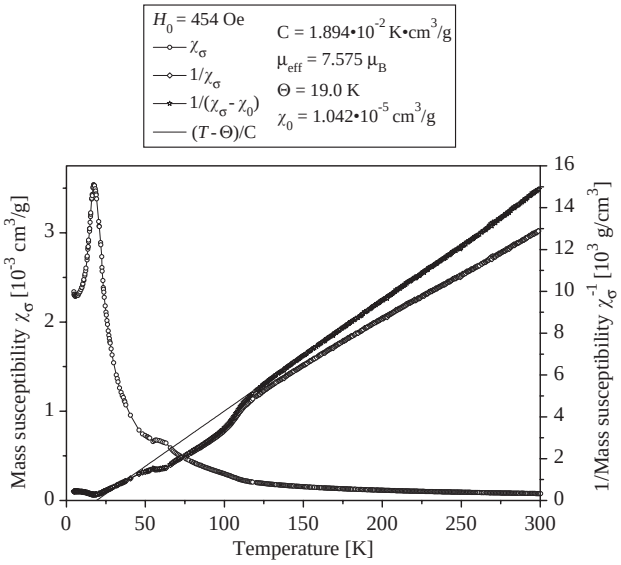

Fig. 2. Temperature dependencies of magnetic susceptibility (left-hand scale) and inverse susceptibility (right-hand scale) as measured with a Cahn RG automatic electrobalance for GdRhSn in an external magnetic field $H_0 = 454$ Oe. In the inset, the magnetic parameters obtained from the fit according to a modified Curie–Weiss law are presented, as explained in the text.

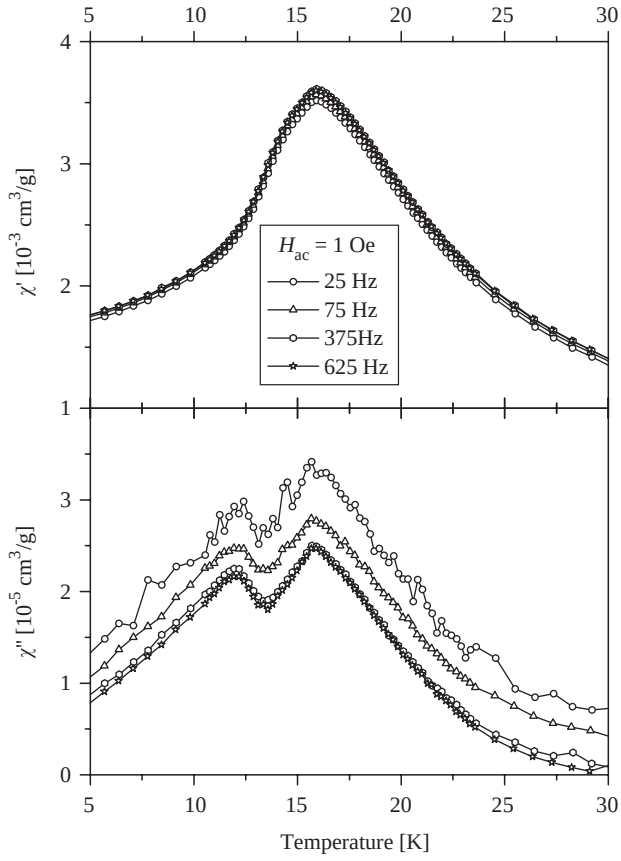

Fig. 3. GdRhSn zero-field susceptibilities χ' and χ'' recorded simultaneously as a function of temperature with an amplitude of the oscillating field $H_{AC} = 1$ Oe at the internal frequencies ranging from $f = 25$ to 625 Hz.

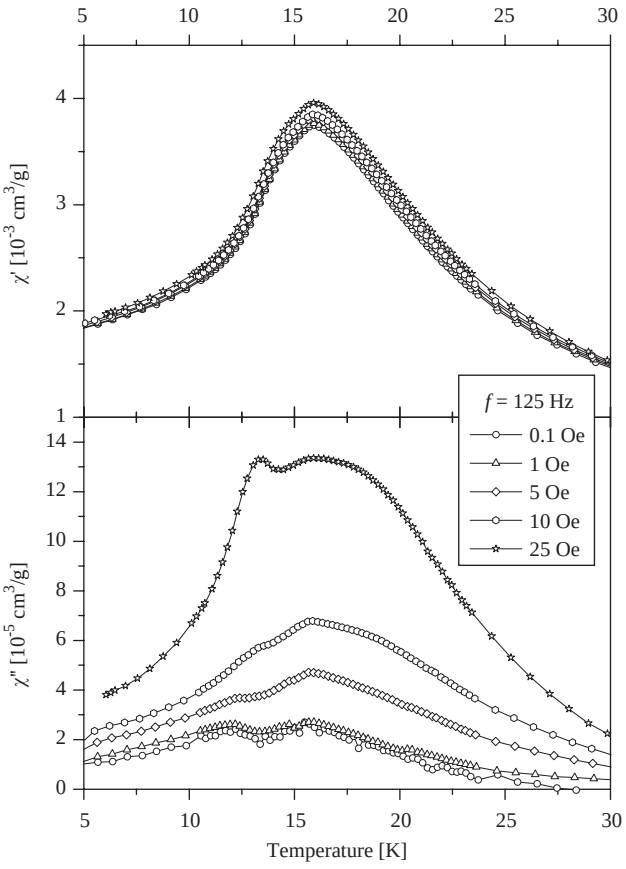

Fig. 4. GdRhSn zero-field susceptibilities χ' and χ'' recorded simultaneously as a function of temperature with different amplitudes of oscillating fields H_{AC} at an internal frequency $f = 125$ Hz.

$\chi_0 = 1.042 \times 10^{-5}$ cm^3/g, the Curie constant $C = 1.894 \times 10^{-2}$ K $*$ cm^3/g, and the paramagnetic Curie temperature $\Theta_p = 19.0$ K. The positive paramagnetic Θ_p Curie temperature indicates a dominant ferromagnetic exchange interaction among the gadolinium atoms [48] and indeed, the presence of such interactions is further confirmed. The effective magnetic moment was derived from the formula $\mu_{eff} = 2.83(MC)^{1/2}$ where M is the molar mass. The experimental value $\mu_{eff} = 7.58\,\mu_B$ is slightly reduced with respect to the theoretical free-ion value $\mu_{eff} = g\,\mu_B[J(J+1)]^{1/2} = 7.94\mu_B$ for the free Gd^{3+} ion.

In order to get more information on the nature of the observed antiferromagnetic transition, additional measurements in AC and DC modes were undertaken using a Lake Shore 7225 apparatus and the results are presented in Figs. 3–12.

The AC method is very well suited for a precise determination of magnetic phase transitions and their dynamics. Especially, AC investigations carried out under ZFC condition with small frequencies f and amplitudes of the oscillating field H_{AC} do not disturb a magnetic system very much, thus, providing an accurate

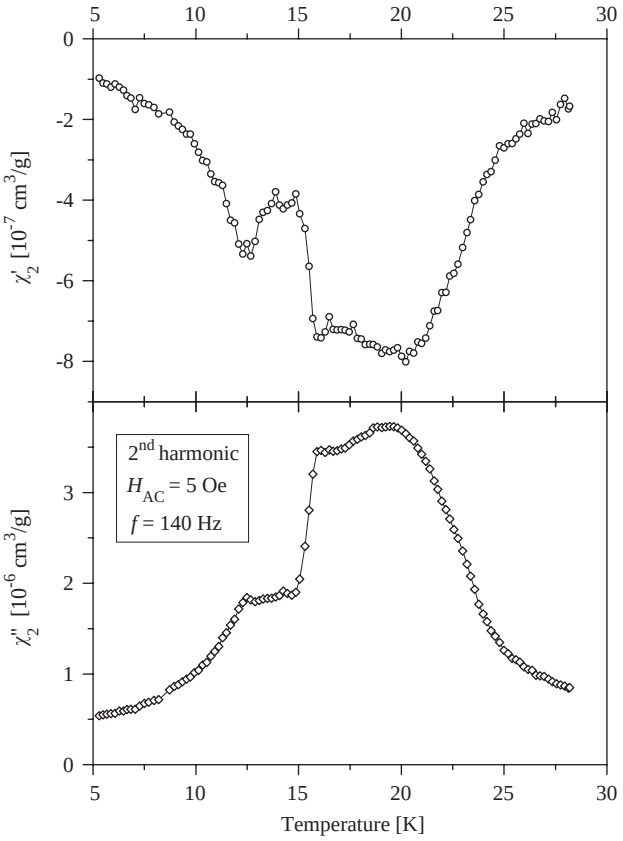

Fig. 5. Temperature dependencies of the signal intensities of the 2nd harmonics χ_2' and χ_2'', respectively, registered with an internal frequency of 140 Hz for GdRhSn. Data were collected after the ZFC process with an oscillating field $H_{AC} = 5$ Oe.

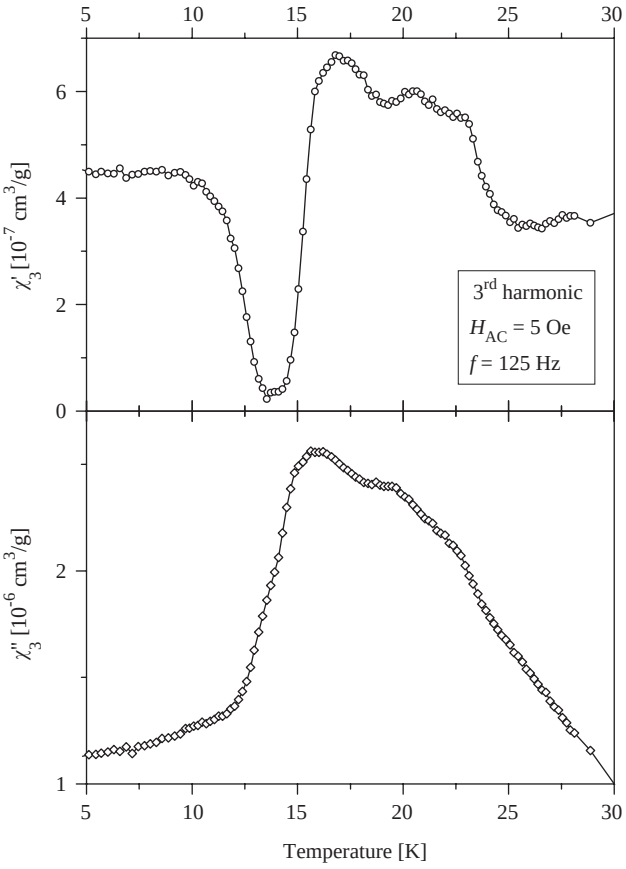

Fig. 6. Temperature dependencies of the signal intensities of the 3rd harmonics χ_3' and χ_3'', respectively, registered with an internal frequency of 125 Hz for GdRhSn. Data were collected after the ZFC process with an oscillating field $H_{AC} = 5$ Oe.

determination of the magnetic phase transition temperatures. The ZFC temperature dependencies of in-phase and out-of-phase susceptibilities $\chi'(f,T)$ and $\chi''(f,T)$ recorded for a number of frequencies f (25–625 Hz with $H_{AC} = 1$ Oe), and amplitudes H_{AC} (0.1–25 Oe with $f = 125$ Hz) are shown in Figs. 3 and 4, respectively. The position of the individual χ' maxima at $T = 16.0(1)$ K do not change with rising f or H_{AC} and it was taken as a measure of the antiferromagnetic phase transition temperature T_N. It agrees perfectly well with that derived from balance measurements. There is no big influence of the frequency f or the oscillating field amplitude H_{AC} on the real part χ' of the magnetic susceptibility in contrast to that observed for the imaginary part χ'' that reflects different energy losses in the magnetically ordered system depending on f or H_{AC}. Such losses are characteristic for systems with a net magnetic moment (i.e. for example ferromagnetic, ferrimagnetic, or canted systems [49], spin glasses or cluster glasses [50–54]). Therefore this observation is a hint that antiferromagnetic ordering in GdRhSn is not simple and surely not a collinear one. This fact is fully supported by the non-vanishing anomalies registered around 16 K in the second χ_2, third χ_3, and fifth χ_5 harmonics of magnetic susceptibility shown in Figs. 5–7, respectively, and further corroborated by the ^{119}Sn and ^{155}Gd Mössbauer data.

The main goal of DC magnetic susceptibility studies was to follow thermal magnetic irreversibilities of the GdRhSn sample as revealed by the ZFC and FC measurements (Figs. 8–12) depending on the strength of the external magnetic field H_0. In limits of experimental errors, the external field H_0 with strength of 100 Oe or 1 kOe has no influence on the temperature of the antiferromagnetic transition represented by the maximum of the respective ZFC $\chi_\sigma(T)$ dependencies (Figs. 8 and 11). However, thermomagnetic irreversibilities for both applied external field values are clearly visible in Figs. 9 and 10 where the FC and ZFC mass susceptibilities χ_σ vs. temperature are displayed (Figs. 9a and 10a) together with their differences i.e. $[(\chi_\sigma(T))_{FC} - \chi_\sigma(T))_{ZFC}]$ (Figs. 9b and 10b). The change of the slope observed systematically below 120 K on the reciprocal magnetic susceptibilities (Figs. 2, 9a, and 10a), and non-zero $[(\chi_\sigma(T))_{FC} - \chi_\sigma(T))_{ZFC}]$ differences revealed above T_N (Figs. 9b, and 10b) could be tentatively ascribed to a small amount of a magnetic

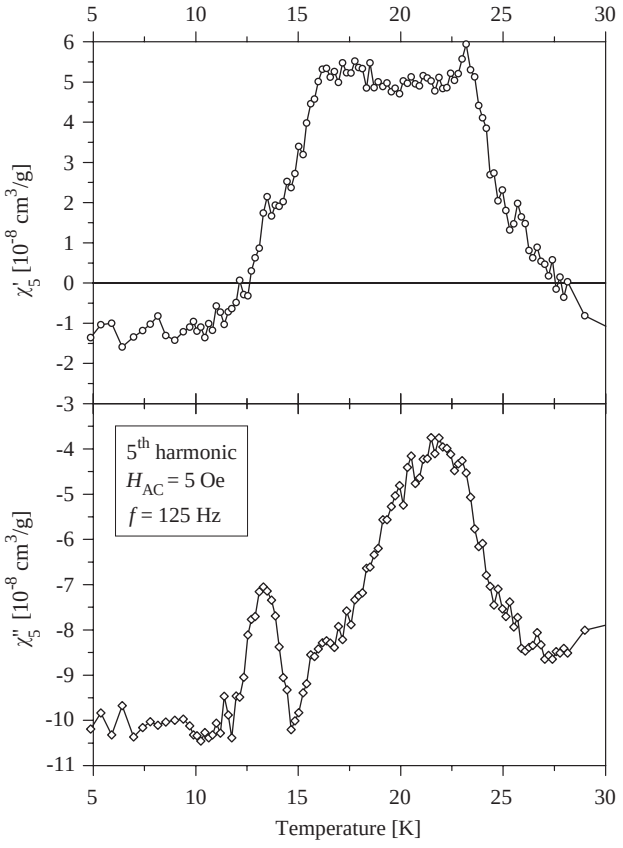

Fig. 7. Temperature dependencies of the signal intensities of the 5th harmonics χ_5' and χ_5'', respectively, registered with an internal frequency of 125 Hz for GdRhSn. Data were collected after the ZFC process with an oscillating field $H_{AC} = 5$ Oe.

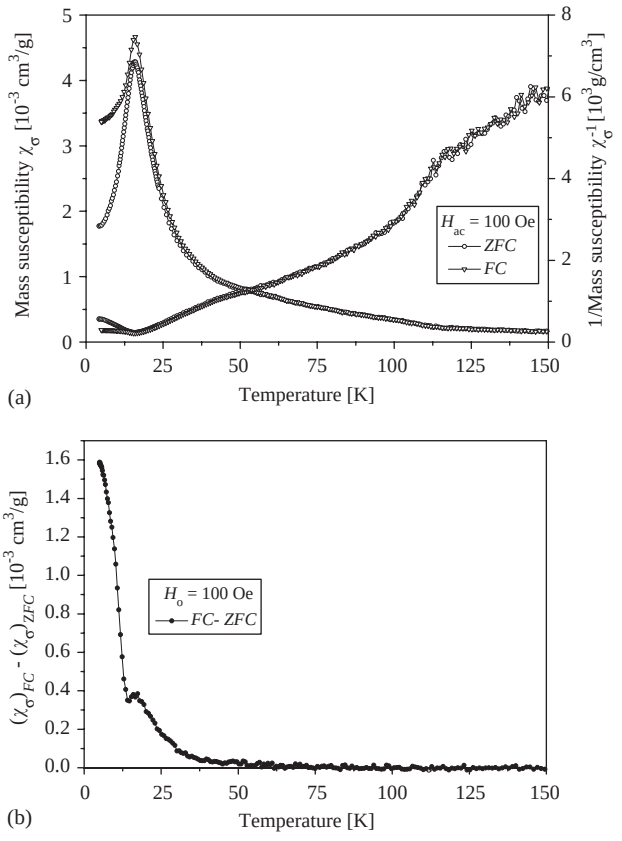

Fig. 9. (a) Zero-field cooled (ZFC) and field-cooled (FC) DC mass susceptibilities χ_σ measured in a static field $H_0 = 100$ Oe as a function of temperature for GdRhSn. (b) Temperature variations of differences between FC and ZFC mass susceptibilities i.e. $[(\chi_\sigma(T))_{FC} - \chi_\sigma(T))_{ZFC}]$.

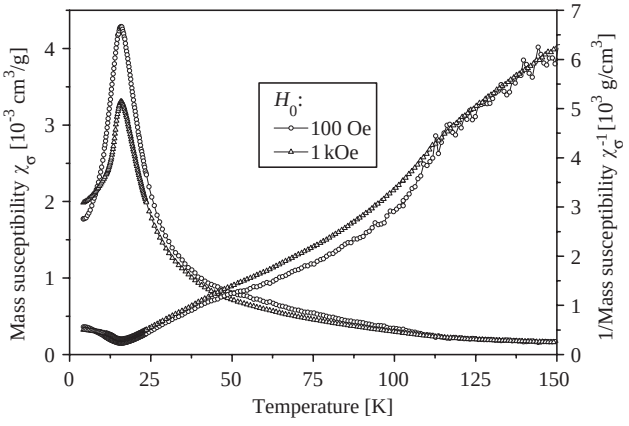

Fig. 8. Plots of zero-field cooled (ZFC) mass susceptibilities χ_σ measured for GdRhSn in static fields $H_0 = 100$ Oe and 1 kOe, respectively, as a function of temperature.

impurity of unknown origin or to a magnetic inhomogeneity of the studied sample. It is worth noting, however, that no impurity has been detected by X-ray diffraction and scanning electron microscopy studies within sensitivities of these techniques. With rising external magnetic field H_0 the maximum of $\chi_\sigma(T)$ strongly decreases and shifts towards lower temperatures (Fig. 11). The mass magnetizations $\sigma(H_0)$ measured for GdRhSn at different temperatures $T = 4.3$, 16, and 25 K, in fields up to 57.5 kOe are shown in Fig. 12. The course of these magnetization curves is similar to that observed for isotypic antiferromagnetic TbNiAl [55,56]. The nonlinear, *S*-shaped character of the magnetizations obtained for temperatures below T_N suggest the existence of ferro- or ferrimagnetic interactions. The value of the magnetic moment at the highest applied field $H_0 = 57.5$ kOe at $T = 4.2$ K is 66.2 Oe cm^3 g^{-1} or 4.49 μ_B being far from the theoretical saturation moment of Gd ($\mu_{sat} = 7\,\mu_B$) in the ordered state. Although, one cannot forget here that this moment has been found from magnetization measurements made on polycrystalline sample, however, it should not play essential role since magnetic anisotropy of Gd intermetallics is usually small. These facts point to a more complex than the simple antiferromagnetic ordering with a non-collinear magnetic arrangement of the gadolinium magnetic moments.

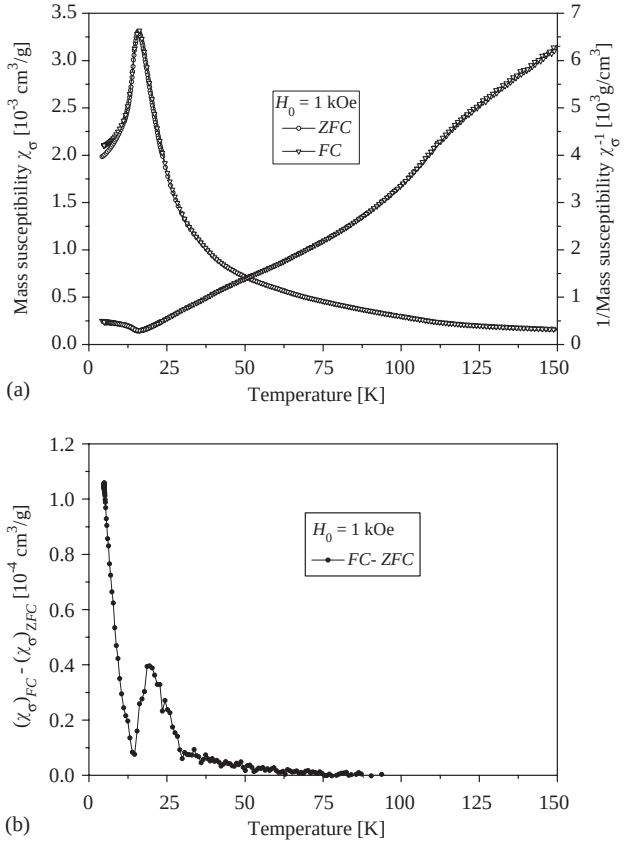

Fig. 10. (a) Zero-field cooled (ZFC) and field-cooled (FC) DC mass susceptibilities χ_σ measured in a static field $H_0 = 1$ kOe as a function of temperature for GdRhSn. (b) Temperature variations of differences between FC and ZFC mass susceptibilities i.e. $[(\chi_\sigma(T))_{FC} - \chi_\sigma(T))_{ZFC}]$.

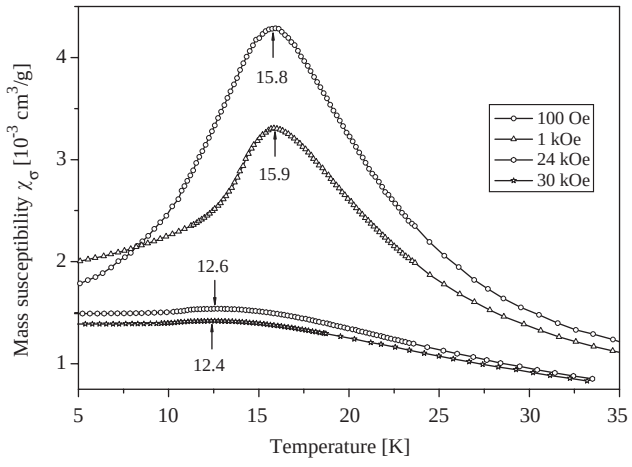

Fig. 11. Zero-field cooled (ZFC) DC mass susceptibilities χ_σ measured for GdRhSn in different static fields H_0 as a function of temperature.

Such a non-collinearity can be associated with the triangular coordination formed by the nearest neighbor gadolinium atoms which leads in a natural way, due to antiferromagnetic coupling in GdRhSn, to frustration of magnetic spins.

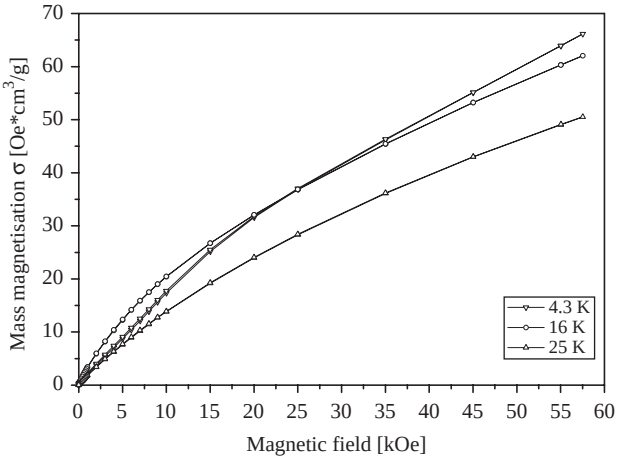

Fig. 12. Mass magnetizations σ measured for GdRhSn at different temperatures $T = 4.3$, 16 and 25 K, respectively. The measurements were always started after zero-field cooling of the sample.

3.3. ^{155}Gd and ^{119}Sn Mössbauer spectroscopy

3.3.1. ^{155}Gd Mössbauer results

3.3.1.1. Resonance spectrum above T_N. The ^{155}Gd resonance spectrum of GdRhSn obtained in the paramagnetic phase is shown in Fig. 13 (top). The spectrum shows a quadrupole splitting and could be fitted with a single component. The sign of the quadrupole interaction is constant in the nuclear ground state, $\Delta E_{Qg} = eV_{zz}Q_g$, and the magnitude of the η-parameter can not be unambiguously determined for this spectrum because of the small magnitude of the excited state quadrupole moment. This causes that the quadrupole splitting of the excited nuclear state ($I_{ex} = 5/2$), which is sensitive to the sign of ΔE_Q and the magnitude of η, is much smaller than the natural linewidth. However, from the overall splitting of the spectrum one can determine a magnitude of the effective quadrupole splitting parameter, $|\Delta E_{Qeff}| = |eV_{zz}Q_g|(1 + 1/3\eta^2)^{1/2}$, which is shown in Table 4 along with other hyperfine parameters.

3.3.1.2. Resonance spectra in the magnetically ordered phase. A typical spectrum measured below the Néel temperature is shown in Fig. 13 (bottom). It clearly indicates that the gadolinium substructure is magnetically ordered. During the fitting procedure the effective quadrupole interaction constant, ΔE_{Qeff}, was fixed to the value obtained in the paramagnetic state while the asymmetry parameter η, and the polar angles θ, φ were varied independently. In addition, the resonance linewidth Γ was fixed to the value obtained from the spectrum taken at 20 K. An attempt to analyze the data with only one component did not give a satisfactory outcome. Only after applying a three-component analysis it was possible to describe the spectrum accurately. During the numerical analysis, special

attention was paid to the estimation of the θ and φ angles. Primarily, the magnitudes of the θ and φ were varied as independent parameters for each magnetic component. The three magnetically split components had different values of the θ (θ_1, θ_2, and θ_3) angles and a common value of the φ angle. In this way, the spectrum taken at 4.2 K yielded the values $\theta_1 = 4(9)^\circ$, $\theta_2 = 131(3)^\circ, \theta_3 = 96(9)^\circ$ and $\varphi = 14(11)^\circ$. The least-squares fitted theoretical function is presented in Fig. 13 by a continuous line. The derived parameters are listed in Table 4.

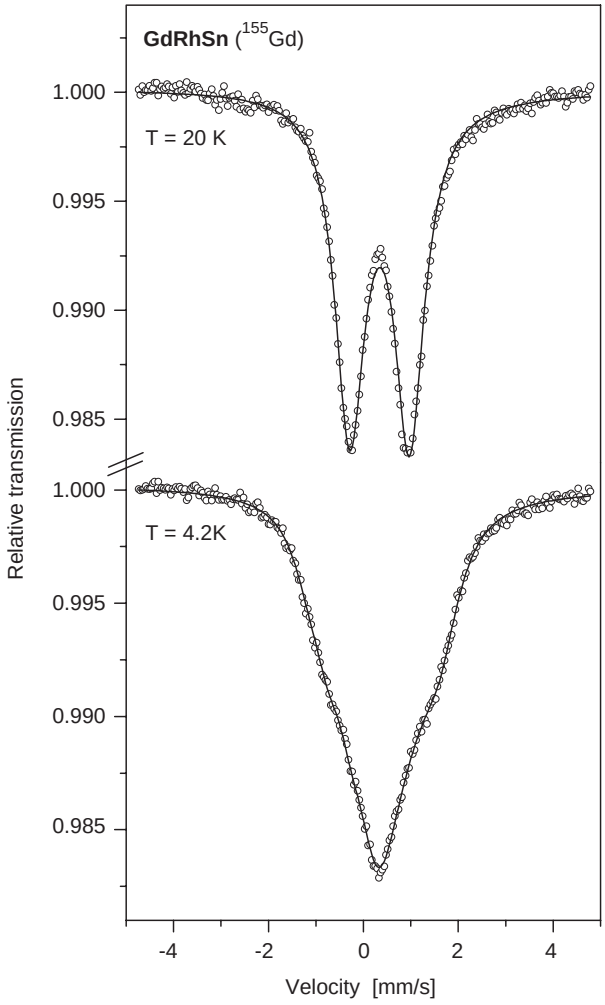

Fig. 13. ^{155}Gd resonance spectra for GdRhSn at $T = 20$ and 4.2 K. The continuous line represents the least-squares fit to the experimental points.

The other spectra in the magnetically ordered regime were analyzed in the same way. The temperature evolution of the H_{hf} field along with the theoretical Gd^{3+} Brillouin function is presented in Fig. 14.

3.3.1.3. Discussion of the ^{155}Gd Mössbauer results. To interpret the Mössbauer data correctly and to get some information on a GdRhSn magnetic structure, one must consider the relation between the local symmetry of the gadolinium site and the hyperfine parameters. The unit cell of GdRhSn contains three formula units with three equivalent gadolinium ions. The only local symmetry elements at the gadolinium sites are two mutually perpendicular mirror planes, where one of the planes lies in the **ab**-basal plane and the second one is parallel to the crystallographic **c**-axis. Due to this arrangement, one of the principal axes of the EFG tensor has to be parallel to the **c**-axis and two others have to lie in the basal plane, with one of them parallel to the cross-section of the mirror planes. With each of the three gadolinium positions in the unit cell are associated, three different principal systems of axes of the EFG tensor, which are equivalent after rotation around the **c**-axis by 120°.

In light of the above considerations the three magnetically split components can be related to the

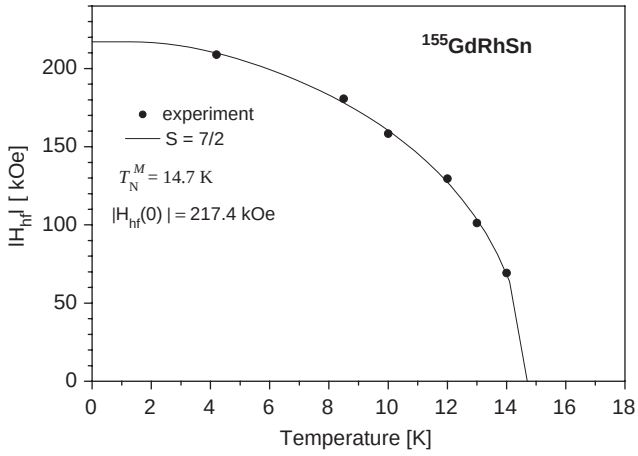

Fig. 14. Temperature evolution of the magnetic hyperfine field $|H_{hf}|$ at the gadolinium site of GdRhSn. The continuous line represents the least-squares fit of the Brillouin function for $S = \frac{7}{2}$. The fit gives the estimated Néel temperature $T_N^M = 14.7$ K and the absolute value of the saturated magnetic hyperfine field $|H_{hf}(0)| = 217.4$ kOe.

Table 4
Hyperfine interaction parameters inferred from the ^{155}Gd resonance spectra obtained for the GdRhSn intermetallic compound at 20 and 4.2 K

T (K)	H_{hf} (kOe)	ΔE_Q** (mm/s)	δ_{is} (mm/s)	η	Γ_A (mm/s)	θ_1 (deg)	θ_2 (deg)	θ_3 (deg)	χ^2
20	—	|2.642(8)|	0.338(2)	—	0.36(1)	—	—	—	1.3
4.2	208(3)	−2.642*	0.351(3)	0.36(6)	0.40(2)	4(9)	131(3)	96(8)	0.83

*Parameter kept constant during the fit.
**Here, $\Delta E_Q = \Delta E_{Q\text{eff}}$ as described in the main text.

three principal axes of the EFG at the gadolinium sites in the unit cell. A single component observed in the paramagnetic state reflects the crystallographic equivalence of the gadolinium position. Generally, for any non-collinear magnetic structure the magnetically split GdRhSn spectrum could be either a single or a multicomponent one. The symmetry of the crystallographic structure determines, however, that any collinear alignment of the gadolinium magnetic moments not parallel to the **c**-axis would give three different components in the magnetically split Mössbauer spectra. The spectra would have the same intensities, magnitudes of H_{hf}, ΔE_Q, δ_{is}, and η parameters but different θ and φ angles. In the case when all the gadolinium magnetic moments were parallel to the crystallographic **c**-axis, one would expect just a single component in the resonance spectrum.

To go further with the discussion on the possible gadolinium magnetic structure one would need to know the exact orientation of the principal axes system of the EFG tensor in the crystallographic structure. Unfortunately, it is not possible to tell from the Mössbauer data alone, the unique orientation of the principal axes of the EFG tensor. However, the Mössbauer results could be interpreted in a relatively simple way if the V_{zz} axis were within the **ab**-basal plane and the V_{yy} axis pointed along the **c**-axis. That particular choice of the alignment of the principal axes system could be supported by the results of detailed Mössbauer studies of the isostructural aluminides GdNiAl and $Gd_{0.10}Tb_{0.90}NiAl$ [57,58]. In that instance the derived value of $\varphi \approx 0$ would imply that the directions of the gadolinium magnetic hyperfine fields would be close to or within the **ab**-basal plane. Thus, we could confine our further discussion to the cases with a planar magnetic order. Provided that the principal V_{zz} axis lies in the basal plane it has to be parallel or perpendicular to the cross-section of the mirror planes. Thus, we can come up with two corresponding magnetic structures which are shown in Fig. 15. In both cases the two gadolinium magnetic moments are collinear while the third one points in another direction. Since the gadolinium sites are arranged in the triangle-like arrangement one can expect a frustration of the antiferromagnetic coupling among the gadolinium magnetic moments. Thus, the third and tilted gadolinium magnetic moment could account for that phenomenon.

The isomer shift δ_{is} can be expressed by the formula: $\delta_{is} \sim \Delta\langle r^2\rangle_{nucl}(|\psi_A^2| - |\psi_S|^2)$, where $\Delta < r^2 >_{nucl}$ is the difference between the mean-square nuclear radii and $|\psi_A|^2$, $|\psi_S|^2$ denote electron densities at the nucleus site of the absorber and the source, respectively. Keeping in mind that for ^{155}Gd the sign of the factor $\Delta\langle r^2\rangle_{nucl}$ is negative [59], then shifts of δ_{is} towards positive values require a reduction of electron densities $|\psi_A|^2$ if the same source is used. Such a reduction can arise from a reduced population of 6*s* states at the gadolinium nuclei, from an increased population of 5*d* states, or from a 6*s* to 5*d* transfer. In this context it is of worth to note that in contrary, if for example the population of 5*d* states decreases owing to a *d* electron transfer from the gadolinium site to the neighboring atoms, then automatically the shielding of gadolinium *s* electrons decreases leading to an increase of their density at the gadolinium site and consequently the isomer shift δ_{is} diminishes. A second reason for a change of δ_{is} is an atomic volume change. A decrease of the atomic volume results in an increase of the corresponding δ_{is}. Obviously, this effect can be excluded when comparing δ_{is} for two isotypic gadolinium compounds of the same volume. In the GdRhSn structure the nearest neighbors to a given gadolinium atom are 4 Rh1 and 1 Rh2 atoms

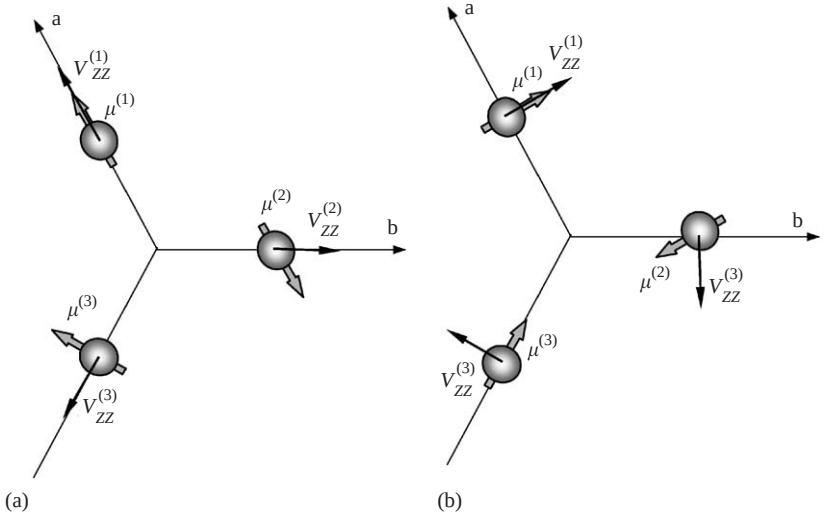

Fig. 15. Two possible magnetic ordering schemes of the gadolinium magnetic moments for GdRhSn below T_N, which are consistent with the Mössbauer results. For explanation see the discussion in the main text.

(see Table 3, and Fig. 1) and the possible transfer of d electrons from the gadolinium to the rhodium sites may be decisive for the final value of the isomer shift δ_{is}. Experimental results have shown indeed, that such a mechanism of d electron transfer really works in establishing mutual isomer shift values [27–31]. In view of the above discussion, one can also note here, that comparable values of isomer shifts observed at $T = 4.2\,K$ for GdRhSn ($\delta_{is} = 0.351(3)\,mm/s$; Table 4), GdAuCd ($\delta_{is} = 0.337(4)\,mm/s$) [31], and GdAuIn ($\delta_{is} = 0.355(4)\,mm/s$) [27] mean simultaneously comparable s electron densities at the gadolinium sites in these compounds.

Since the trivalent gadolinium ions are in $^8S_{7/2}$ electronic states with a spherical distribution of the $4f$ electronic charge, only the lattice term contributes to the magnitude of V_{zz} in the rare earth site. Hence, the determination of the sign and magnitude of $\Delta E_Q = eV_{zz}Q$ at the gadolinium site together with the asymmetry parameter η allow to estimate the quadrupolar terms B_2^0 and B_2^2 in the Stevens expansion of the crystal field *Hamiltonian* $\Sigma B_n^m O_n^m$, as they are directly related by two simple formulae

$$B_2^0[K] = -\alpha_J * \langle r^2 \rangle_{4f} * 90.2 * \Delta E_Q(^{155}Gd),$$

$$B_2^2 = \eta B_2^0.$$

Here, α_J is the appropriate Stevens factor, the mean squared radius of the $4f$ wave function $\langle r^2 \rangle_{4f}$ is expressed in atomic units and ΔE_Q in mm/s ($\Delta E_Q = -2.642\,mm/s$; see Table 4). If B_2^0 is the leading term in the crystal field Hamiltonian then its sign gives information about the single ion magnetic anisotropy. Since the measured ΔE_Q is negative, one should expect, for example, a positive value of B_2^0 for isostructural *RE*RhSn compounds with heavy rare earth like Er, Tm, and Yb ($\alpha_J > 0$), and a negative value of B_2^0 for compounds with light rare earths like Ce, Nd, Pr ($\alpha_J < 0$). In turn, for a positive value of the B_2^0 parameter the basal plane ($\perp z$) is preferred for the moment direction while for a negative value an ordering along the z-axis is anticipated [60–62].

The temperature dependence of the magnetic hyperfine field $|H_{hf}(T)|$ (Fig. 14) can be well described in the frame of molecular field approximation by a Brillouin function with $S = \frac{7}{2}$. The resulting fit gives the estimation for the Néel temperature $T_N^M = 14.7\,K$ which is only slightly smaller than that obtained from magnetic AC measurements $T_N = 16\,K$. The absolute value of the saturated magnetic hyperfine field $|H_{hf}(0)|$ is 217.4 kOe. Assuming that the latter value is negative as observed for gadolinium intermetallics and neglecting to a first approximation the orbital as well as the dipolar contributions to the magnetic hyperfine field H_{hf} at the gadolinium site, one can estimate the contribution coming from the conduction electron polarization H_{CE}. Following the discussion presented in [63] one can show that in the above-mentioned approximation $H_{CE} = H_{hf} - H_{CP}$, where $H_{CP} = -340(20)\,kOe$ [64,65] is the field due to core polarization by the local $4f$ moment. Taking all of that into account, one obtains finally a positive $H_{CE} = H_{hf} - H_{CP} = -217.4\,kOe - (-340\,kOe) = 122.6\,kOe$.

3.3.2. ^{119}Sn Mössbauer results

The ^{119}Sn Mössbauer spectra were taken both in the paramagnetic and magnetically ordered states. Here, because of a poor resolution and relatively small magnetic splitting of the spectra obtained below T_N, the asymmetry parameter $\eta = V_{xx} - V_{yy}/V_{zz}$ was fixed zero during all performed fits.

Typical ^{119}Sn spectra are shown in Fig. 16. In order to get an accurate description of the spectra detected both below and above T_N, the second non-magnetically split

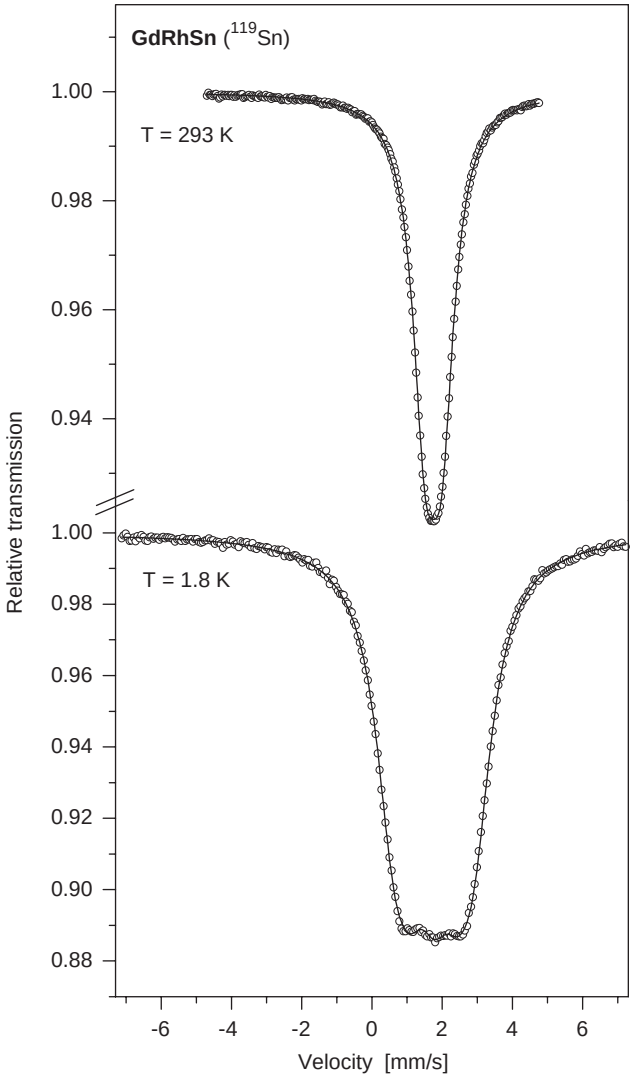

Fig. 16. ^{119}Sn resonance spectra for GdRhSn obtained at 293 and 1.8 K. The continuous lines represent the least-squares fits to the experimental points.

Table 5
Hyperfine interaction parameters inferred from the ^{119}Sn resonance spectra obtained for GdRhSn at the lowest temperature 1.8 K as indicated and at room temperature (293 K)

T (K)	H_{hf} (kOe)	$\Delta E_Q = eV_{zz}Q$ (mm/s)	δ_{is} (mm/s)	Γ (mm/s)	θ (deg)	AR (%)	χ^2
1.8	15.1(1)	0.997*	1.762(2)	1.26(1)	54(1)	89	0.89
	—	0.46(6)	1.762(2)	0.9*	—	11	
293	—	|0.997(4)|	1.751(2)	0.86(1)	—	89*	1.69
		0.46*	1.751(2)	0.9*		11*	

*Parameter kept constant during the fit.

component having a smaller quadrupole interaction constant (Table 5) with intensity of about 11% (taken from area ratio at 1.8 K, see Table 5) was always included in the fitting procedure. The first component, with an 89% area ratio, was assigned to the tin atoms occupying their proper sites in the crystallographic structure. The second one might arise from tin atoms that swap their positions with the rhodium atoms. Although the single crystal data gave no hint for Sn/Rh mixing, this is possible in the polycrystalline bulk material.

The spectrum recorded at 1.8 K showing relatively weak and rather featureless magnetic splitting was effectively fitted with one θ value (see Table 5). The derived value for the magnetic hyperfine magnetic field $H_{hf} = 15.1(1)$ kOe is much higher than that found by Dwight [1] i.e. $H_{hf} = 3.9$ kOe at 4.2 K.

In contrast to gadolinium, a tin atom does not have its own magnetic moment. A magnetic hyperfine field at the tin nucleus is induced solely by the other magnetic moments in the tin neighborhood. Usually, a transferred magnetic hyperfine field at the tin site can be treated as a good measure of a net magnetic moment of the tin neighbors. Like in the ^{155}Gd case an interpretation of the ^{119}Sn data requires a closer look at the local crystallographic structure of the tin site ($m2m$). Characteristic features of the GdRhSn structure are the Gd–Rh and Sn–Rh planes stacked along the c-axis. Thus, the tin atoms are placed exactly in the middle between Gd–Rh planes. That kind of local tin symmetry means that for any type of antiferromagnetic ordering with antiferromagnetically coupled Gd–Rh planes ^{119}Sn spectra would not show any magnetic splitting at all. The small magnetic hyperfine fields and the smeared out ^{119}Sn magnetic spectra could suggest that the Gd–Rh planes are generally coupled antiferromagnetically, however, with some local disturbances. These local disturbances could originate again from the frustration of the antiferromagnetic coupling in the triangular gadolinium substructure that has already been suggested by the ^{155}Gd MS as well as the magnetic results.

The value of the tin isomer shift ($\delta_{is} = 1.75$ mm/s-1.76 mm/s, see Table 5) does not depend on the temperature remarkably and is typical for that of tin in other intermetallic systems as, for example, observed in the stannides GdTSn (T = Au, Ag) [66].

4. Conclusions

The equiatomic stannide GdRhSn has been studied by several experimental methods involving X-ray diffraction, magnetization, and magnetic susceptibility measurements as well as MS with ^{119}Sn and ^{155}Gd isotopes. GdRhSn crystallizes with the ZrNiAl type, space group $P\bar{6}2m$. Precise AC magnetic susceptibility measurements showed that GdRhSn undergoes an antiferromagnetic transition at $T_N = 16.0(1)$ K being in very good agreement with the transition temperatures derived from other methods applied. Analysis of the hyperfine parameters obtained from MS for both isotopes has delivered much valuable information on the electronic and structural properties. The value of the ^{119}Sn isomer shift at 1.8 K is 1.76 mm/s and the value of the ^{155}Gd isomer shift offers deeper insight into the electron densities in GdRhSn as discussed in the main text. The magnetic anisotropy in isostructural RERhSn compounds has been presented in view of the negative quadrupole interaction constant ΔE_Q obtained from ^{155}Gd MS.

All obtained results can be interpreted in a self-consistent way only if the magnetic structure of GdRhSn is not collinear. It is postulated that the main reason for the lack of collinearity is spin frustration resulting from the topology of the crystal structure where the nearest neighbor gadolinium magnetic moments form a triangular-like arrangement with antiferromagnetic coupling. Two models of possible gadolinium magnetic moment arrangements which are supported by the experimental data have been proposed.

Acknowledgments

We are grateful to the Degussa-Hüls A.G. for a gift of rhodium powder and to H. J. Göcke for the work at the scanning electron microscope. This work was supported

by the Deutsche Forschungsgemeinschaft through SPP 1166 *Lanthanoidspezifische Funktionalitäten in Molekül und Material* and by Poland's Committee for Scientific Research grant under Contract no: 1 P03B 084 28. K.L. is indebted to the Deutsche Forschungsgemeinschaft for a research grant.

References

[1] A.E. Dwight, W.C. Harper, C.W. Kimball, J. Less-Common Met. 30 (1973) 1.
[2] Ch.D. Routsi, J.K. Yakinthos, E. Gamari-Seale, J. Magn. Magn. Mater. 110 (1992) 317.
[3] Ch.D. Routsi, J.K. Yakinthos, H. Gamari-Seale, J. Magn. Magn. Mater. 117 (1992) 79.
[4] F. Canepa, S. Cirafici, J. Alloys Compd. 232 (1996) 71.
[5] A. Szytuła, B. Penc, E. Ressouche, J. Alloys Compd. 244 (1996) 94.
[6] A. Szytuła, Lithuanian J. Phys. 37 (1997) 32.
[7] A.E. Dwight, J. Less-Common Met. 34 (1974) 279.
[8] D. Kaczorowski, A. Leithe-Jasper, P. Rogl, H. Flandorfer, T. Cichorek, R. Pietri, B. Andraka, Phys. Rev. B 60 (1999) 422.
[9] K. Katoh, G. Terui, Y. Niide, H. Aoki, A. Ochiai, Physica B 259–261 (1999) 161.
[10] O. Trovarelli, C. Geibel, R. Cardoso, S. Mederle, R. Borth, B. Buschinger, F.M. Grosche, Y. Grin, G. Sparn, F. Steglich, Phys. Rev. B 61 (2000) 9467.
[11] R. Pietri, B. Andraka, D. Kaczorowski, A. Leithe-Jasper, P. Rogl, Phys. Rev. B 61 (2000) 12169.
[12] B. Andraka, R. Pietri, D. Kaczorowski, A. Leithe-Jasper, P. Rogl, J. Appl. Phys. 87 (2000) 5149.
[13] Y. Bando, T. Suemitsu, K. Takagi, H. Tokushima, Y. Echizen, K. Katoh, K. Uemo, Y. Maeda, T. Takabatake, J. Alloys Compd. 313 (2000) 1.
[14] R. Mishra, R. Pöttgen, R.-D. Hoffmann, H. Trill, B.D. Mosel, H. Piotrowski, M.F. Zumdick, Z. Naturforsch. 56b (2001) 589.
[15] A. Ślebarski, M.B. Maple, E.J. Freeman, C. Sirven, M. Radłowska, A. Jezierski, E. Granado, Q. Huang, J.W. Lynn, Philos. Mag. 82B (2002) 943.
[16] A. Ślebarski, N.A. Frederick, M.B. Maple, Philos. Mag. 82B (2002) 1275.
[17] A. Ślebarski, M. Radłowska, T. Zawada, M.B. Maple, A. Jezierski, A. Zygmunt, Phys. Rev. B 66 (2002) 104434.
[18] A. Ślebarski, A. Jezierski, Phys. Stat. Sol. B 236 (2003) 340.
[19] H. Tou, M.S. Kim, T. Takabatake, M. Sera, Phys. Rev. B 70 (2004) 100407.
[20] P.-C. Ho, V.S. Zapf, A. Slebarski, M.B. Maple, Philos. Mag. 84 (2004) 2119.
[21] A. Slebarski, K. Grube, R. Lortz, C. Meingast, H. von Löhneysen, J. Magn. Magn. Mater. 272–276 (2004) 234.
[22] T. Suzuki, H. Higaki, I. Ishii, M.S. Kim, T. Takabatake, J. Magn. Magn. Mater. 272–276 (2004) E35.
[23] M.S. Kim, T. Sasakawa, Y. Echizen, T. Takabatake, Jpn. J. Appl. Phys. 42 (2003) 6512.
[24] M.S. Kim, Y. Echizen, K. Umeo, S. Kobayashi, M. Sera, P.S. Salamakha, O.L. Sologub, T. Takabatake, X. Chen, T. Tayama, T. Sakakibara, M.H. Jung, M.B. Maple, Phys. Rev. B 68 (2003) 054416.
[25] M.S. Kim, Y. Echizen, K. Umeo, T. Tayama, T. Sakakibara, T. Takabatake, Physica B 329–333 (2003) 524.
[26] Y. Echizen, K. Yamane, T. Takabatake, Physica B 329–333 (2003) 522.
[27] R. Pöttgen, G. Kotzyba, E.A. Görlich, K. Łątka, R. Dronskowski, J. Solid State Chem. 141 (1998) 352.
[28] R.-D. Hoffmann, Th. Fickenscher, R. Pöttgen, C. Felser, K. Łątka, R. Kmieć, Solid State Sci. 4 (2002) 609.
[29] K. Łątka, Z. Tomkowicz, R. Kmieć, A.W. Pacyna, R. Mishra, Th. Fickenscher, R.-D. Hoffmann, R. Pöttgen, H. Piotrowski, J. Solid State Chem. 168 (2002) 331.
[30] K. Łątka, R. Kmieć, A.W. Pacyna, Th. Fickenscher, R.-D. Hoffmann, R. Pöttgen, Solid State Sci. 6 (2004) 301.
[31] K. Łątka, R. Kmieć, A.W. Pacyna, Th. Fickenscher, R.-D. Hoffmann, R. Pöttgen, J. Magn. Magn. Mater. 280 (2004) 90.
[32] K. Łątka, R. Kmieć, R. Kruk, A.W. Pacyna, M. Rams, T. Schmidt, R. Pöttgen, Nukleonika 48 (Suppl.) (2003) S35.
[33] R. Pöttgen, Th. Gulden, A. Simon, GIT Labor-Fachzeitschrift 43 (1999) 133.
[34] D. Kußmann, R.-D. Hoffmann, R. Pöttgen, Z. Anorg. Allg. Chem. 624 (1998) 1727.
[35] K. Yvon, W. Jeitschko, E. Parthé, J. Appl. Crystallogr. 10 (1977) 73.
[36] M.F. Zumdick, R.-D. Hoffmann, R. Pöttgen, Z. Naturforsch. 54b (1999) 45.
[37] G.M. Sheldrick, SHELXL-97, Program for Crystal Structure Refinement, University of Göttingen, 1997.
[38] H.D. Flack, G. Bernadinelli, Acta Crystallogr. A 55 (1999) 908.
[39] H.D. Flack, G. Bernadinelli, J. Appl. Crystallogr. 33 (2000) 1143.
[40] G. Czjzek, Kernforschungszentrum Karlsruhe, unpublished.
[41] G.J. Long, T.E. Cranshaw, G. Longworth, Mössbauer Effect Ref. Data J. 6 (1983) 42.
[42] K. Tomala, G. Czjzek, J. Fink, H. Schmidt, Solid State Commun. 24 (1977) 857.
[43] G. Czjzek, Mössbauer Spectroscopy of New Materials Containing Gadolinium, in: G.J. Long, F. Grandjean (Eds.), Mössbauer Spectroscopy Applied to Magnetism and Materials Science, vol. 1, Plenum Press, New York, 1993, p. 373.
[44] H. Armon, E.R. Bauminger, S. Ofer, Phys. Lett. 43B (1973) 380.
[45] W. Henning, G. Baehrle, P. Kienle, Phys. Lett. B 31 (1970) 203.
[46] J. Emsley, The Elements, Clarendon Press, Oxford, 1989.
[47] J. Donohue, The Structures of the Elements, Wiley, New York, 1974.
[48] N.W. Ashcroft, N.D. Mermin, Solid State Physics, Holt, Rinehart and Wilson, New York, 1976.
[49] T. Sato, T. Ando, T. Watanabe, S. Itoh, Y. Endoh, M. Furusaka, Phys. Rev. B 48 (1993) 6074.
[50] K. Binder, Y. Yang, Rev. Mod. Phys. 58 (1986) 801.
[51] H. Maletta, W. Zinn, Spin glasses, in: K.A. Gschneidner Jr., L. Eyring (Eds.), Handbook on the Physics and Chemistry of Rare Earths, vol. 12, North-Holland, Amsterdam, 1989, p. 213.
[52] K.H. Fisher, J.A. Hertz, Spin Glasses, Cambridge University Press, Cambridge, 1991.
[53] P. Nordblad, P. Svedlindh, Experiments on spin glass, in: A.P. Young (Ed.), Series on Directions in Condensed Matter Physics, vol. 12, World Scientific, Singapore, 1998, p. 1.
[54] J.A. Mydosh, Spin Glasses an Experimental Introduction, Taylor & Francis, London, 1993.
[55] G. Ehlers, H. Maletta, Z. Phys. B 99 (1996) 145.
[56] P. Javorský, P. Burlet, V. Sechovský, A.V. Andreev, J. Brown, P. Svoboda, J. Magn. Magn. Mater. 166 (1997) 133.
[57] J. Gurgul, Thesis, Jagiellonian University, Poland, M. Smoluchowski Institute of Physics, 2002.
[58] M. Rams, J. Gurgul, K. Tomala, K. Kmieć, R. Kruk, to be published.
[59] E.R. Bauminger, G.M. Kalvius, F.E. Wagner, Isomer shifts in the rare earth, in: G.K. Shenoy, F.E. Wagner (Eds.), Mössbauer Isomer Shifts, North Holland Publishing Company, Amsterdam, New York, Oxford, 1978, p. 661.
[60] J.E. Greedan, V.U.S. Rao, J. Solid State Chem. 6 (1973) 387.

[61] J. Jensen, A.R. Mackintosch, Rare Earth Magnetism, Clarendon Press, Oxford, 1991.
[62] W.E. Wallace, S.G. Sankar, V.U.S. Rao, Crystal field effects in rare-earth intermetallic compounds, in: J.D. Dunitz, P. Hemmerich, J.A. Ibers, C.K. Jørgensen, J.B. Neilands, D. Reinen, R.J.P. Williams (Eds.), Structure and Bonding, vol. 33, Springer, Berlin, 1997, p. 1.
[63] K. Łątka, R. Kmieć, M. Rams, A.W. Pacyna, V.I. Zaremba, R. Pöttgen, Z. Naturforsch. 59b (2004) 947.
[64] R.E. Watson, A.J. Freeman, Hartree–Fock theory of electric and magnetic hyperfine interactions in atoms and magnetic compounds, in: A.J. Freeman, R.B. Frankel (Eds.), Hyperfine Interactions, Academic Press, New York, 1967, p. 53.
[65] R.E. Gegenwarth, J.I. Budnick, S. Skalski, J.H. Wernick, Phys. Rev. Lett. 18 (1967) 9.
[66] K. Łątka, E.A. Görlich, W. Chajec, R. Kmieć, A.W. Pacyna, J. Alloy Compd. 262–263 (1997) 108.